Supplement of Atmos. Chem. Phys., 18, 8113–8136, 2018
https://doi.org/10.5194/acp-18-8113-2018-supplement


Atmospheric Chemistry and Physics
Open Access
EGU

*Supplement of*

# On the suitability of current atmospheric reanalyses for regional warming studies over China

**Chunlüe Zhou et al.**

*Correspondence to:* Kaicun Wang (kcwang@bnu.edu.cn)

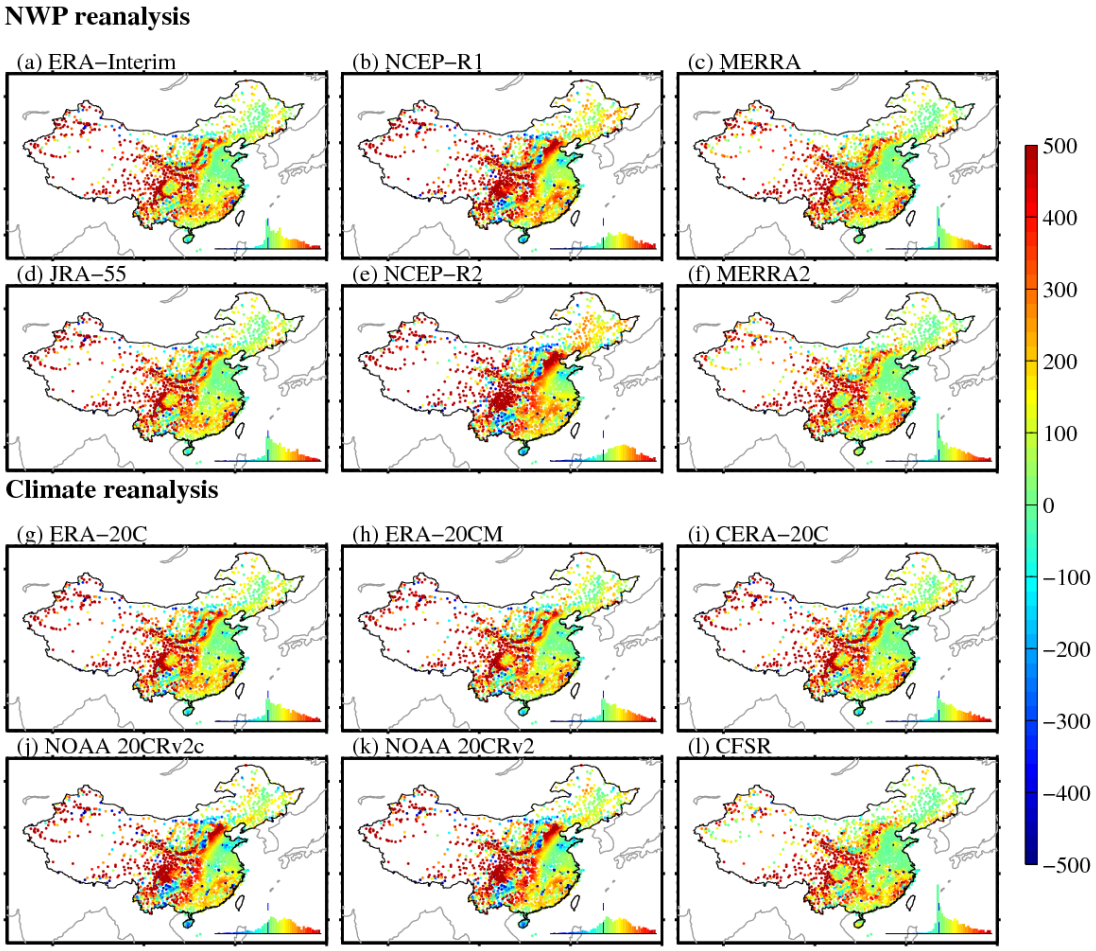


**Figure S1.** The elevation difference (ΔHeight, unit: m) between the model and observation stations. The information on model resolution is included in Table 1.

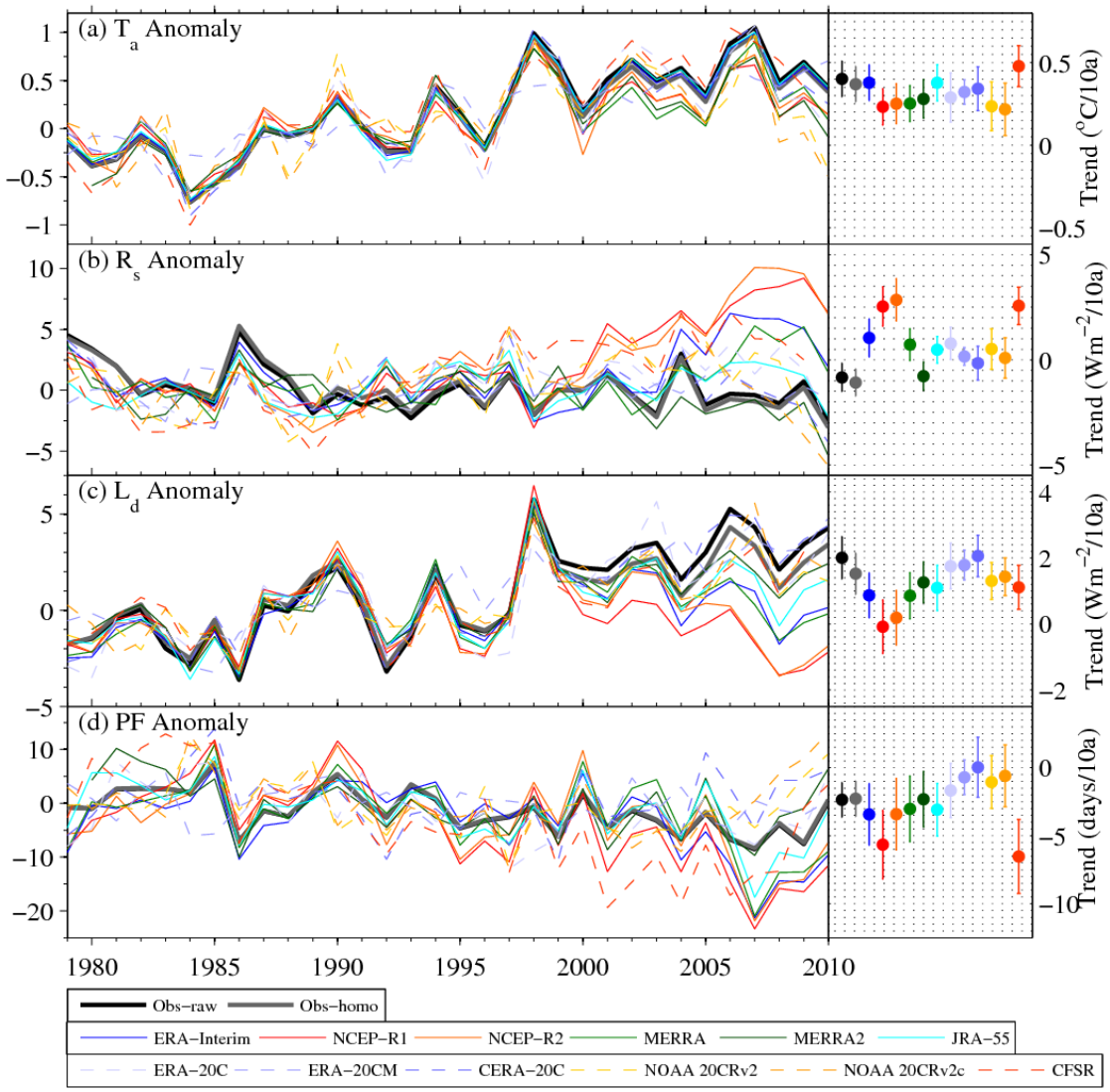


**Figure S2.** The time series of (**a**) surface air temperature anomaly ($T_a$), (**b**) surface incident solar radiation ($R_s$), (**c**) surface downward longwave radiation ($L_d$) and (**d**) precipitation frequency anomaly (PF) with their trends (in right each) from the raw observation, homogeneous observation and the twelve reanalysis products during the period 1979-2010 over China. The error-bars show the 95% confident intervals of the trends.

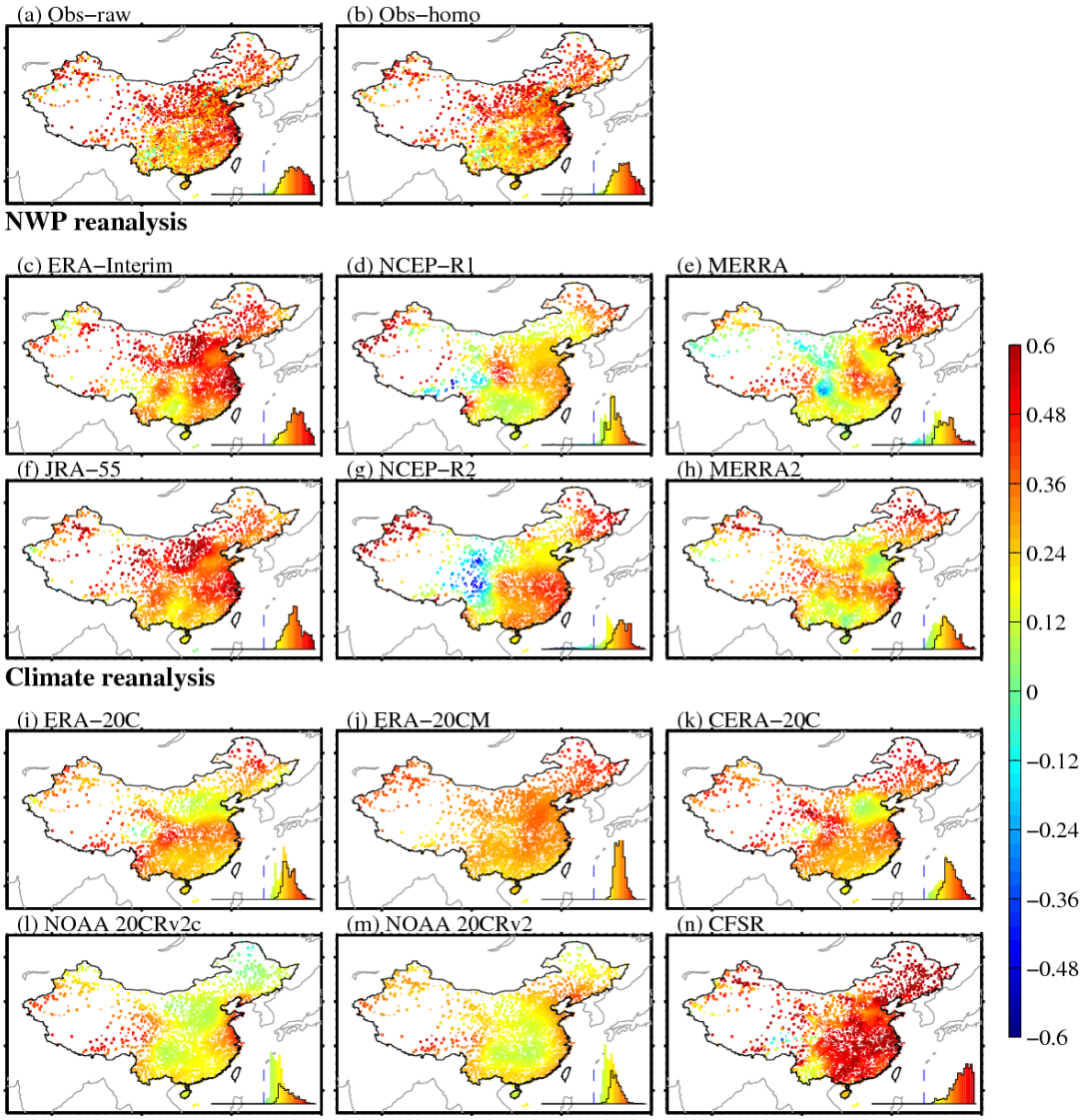


**Figure S3.** The trends in surface air temperature ($T_a$, unit: ℃/decade) during the period 1979-2010 from (**a**) raw observations, (**b**) homogeneous observations and the twelve reanalysis products over China, i.e., (**c**) ERA-Interim, (**d**) NCEP-R1, (**e**) MERRA, (**f**) JRA-55, (**g**) NCEP-R2, (**h**) MERRA2, (**i**) ERA-20C, (**j**) ERA-20CM, (**k**) CERA-20C, (**l**) NOAA 20CRv2c, (**m**) NOAA 20CRv2 and (**n**) CFSR. The probability distribution functions of all the trends are shown as colored histogram, and the black stairs are integrated from the trends with a significance level of 0.05 (based on two-tailed Student's *t*-test).

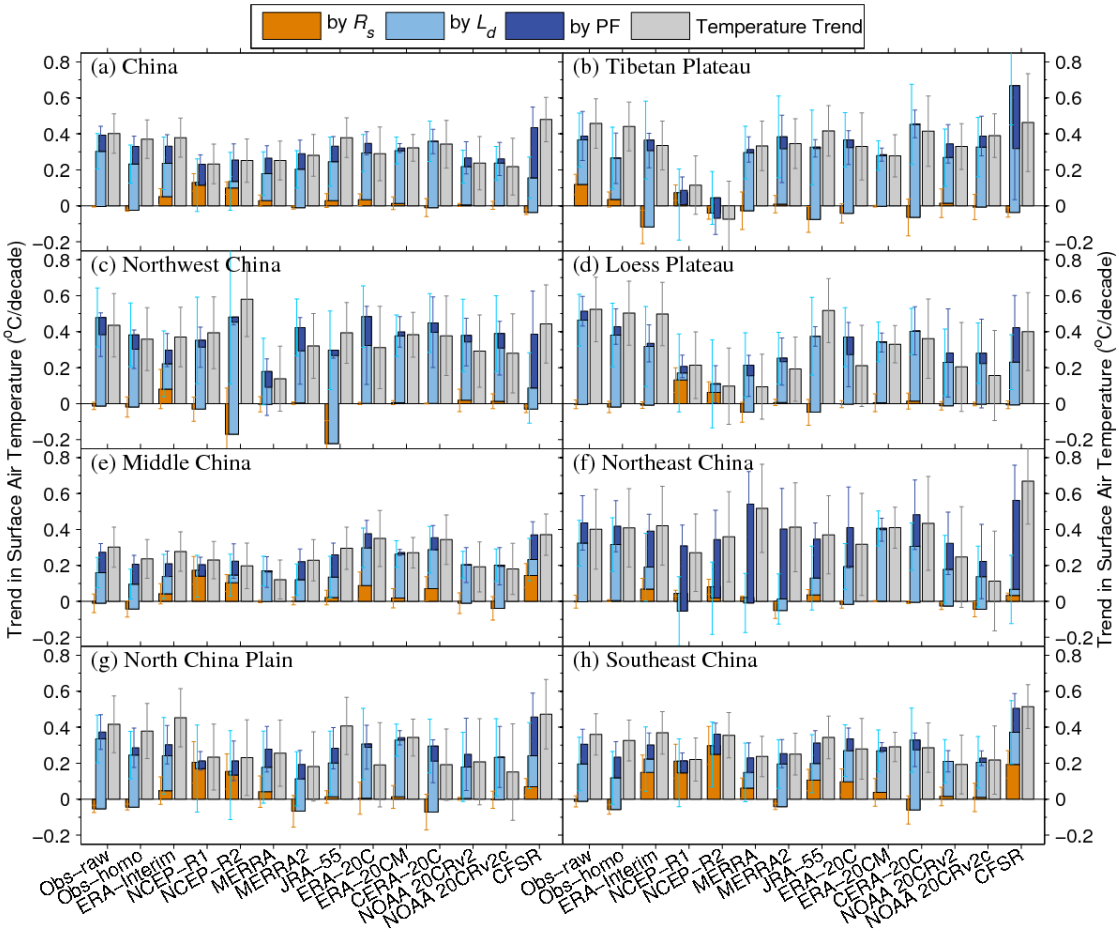


**Figure S4.** Contribution of trends in surface air temperature ($T_a$, unit: ℃/decade) from three relevant parameters, i.e., surface incident solar radiation ($R_s$, in brown, unit: W m$^{-2}$/decade), surface downward longwave radiation ($L_d$, in light blue, unit: W m$^{-2}$/decade) and the precipitation frequency (PF, in deep blue, unit: days/decade) during the period 1979-2010 in the raw observations, homogeneous observations and the twelve reanalysis products over China and its seven subregions.

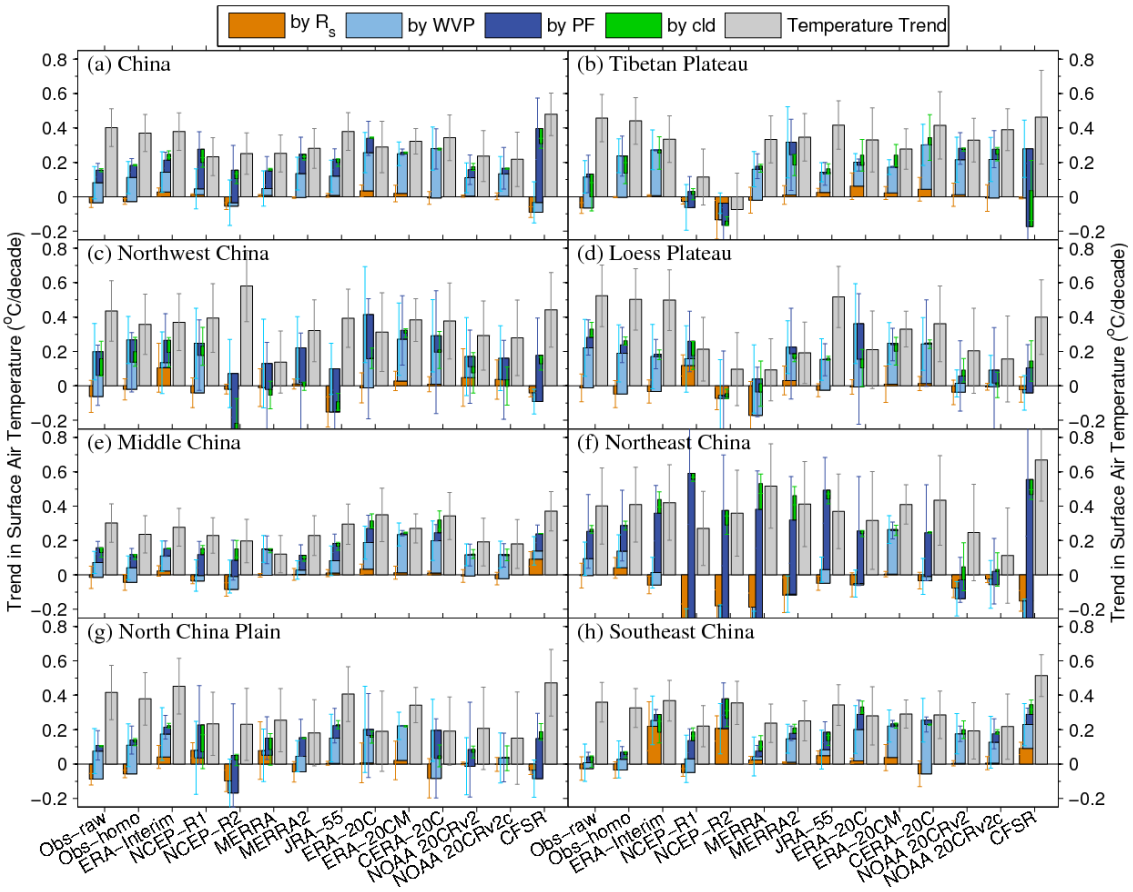


**Figure S5.** The same as Figure S4, but using the atmospheric water vapor and cloud fraction instead of surface downward longwave radiation.

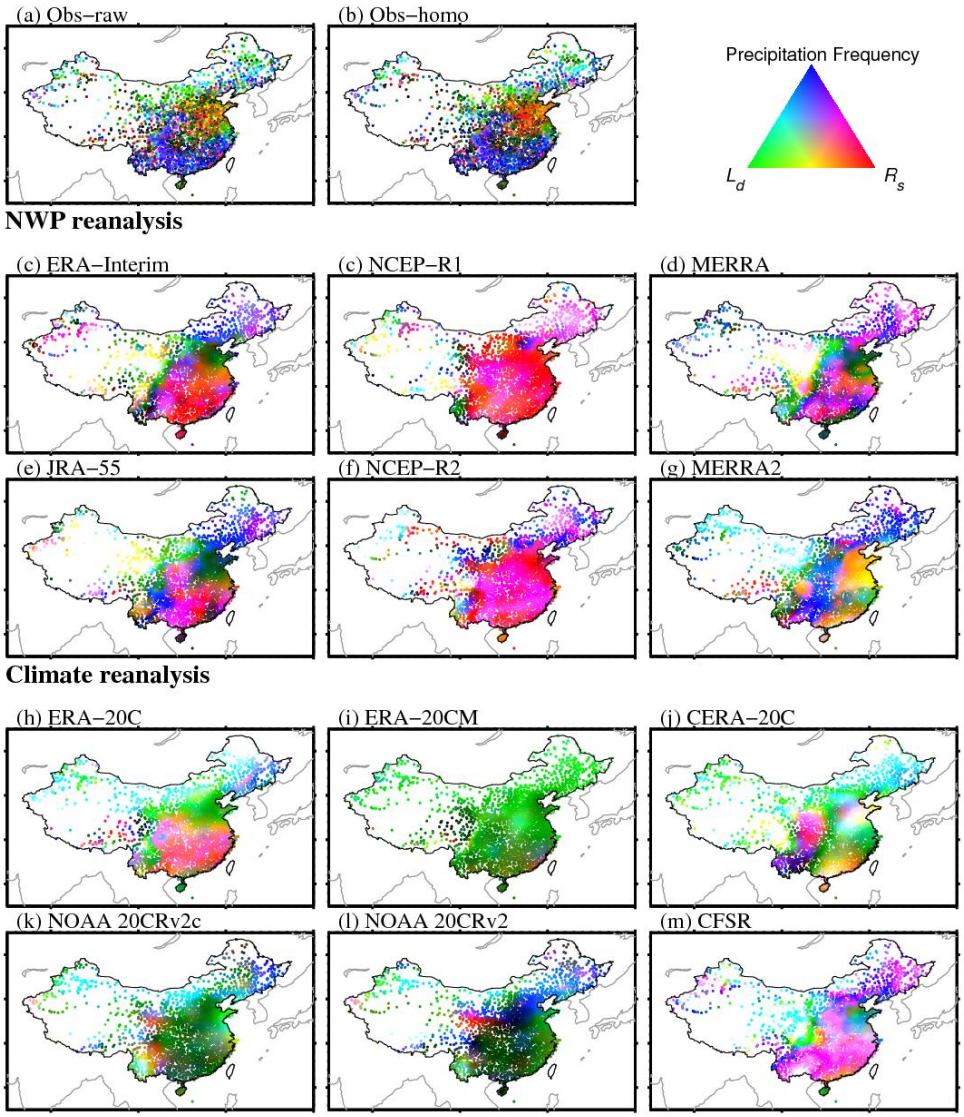


**Figure S6.** Composite map of contribution of trends in three relevant parameters [surface incident solar radiation ($R_s$, in red), surface downward longwave radiation ($L_d$, in green) and the precipitation frequency (in blue)] to trends in surface air temperature ($T_a$, unit: ℃/decade) during the period 1979-2010 from (**a**) the raw observations, (**b**) homogeneous observations and the twelve reanalysis products over China, i.e., (**c**) ERA-Interim, (**d**) NCEP-R1, (**e**) MERRA, (**f**) JRA-55, (**g**) NCEP-R2, (**h**) MERRA2, (**i**) ERA-20C, (**j**) ERA-20CM, (**k**) CERA-20C, (**l**) NOAA 20CRv2c, (**m**) NOAA 20CRv2 and (**n**) CFSR.

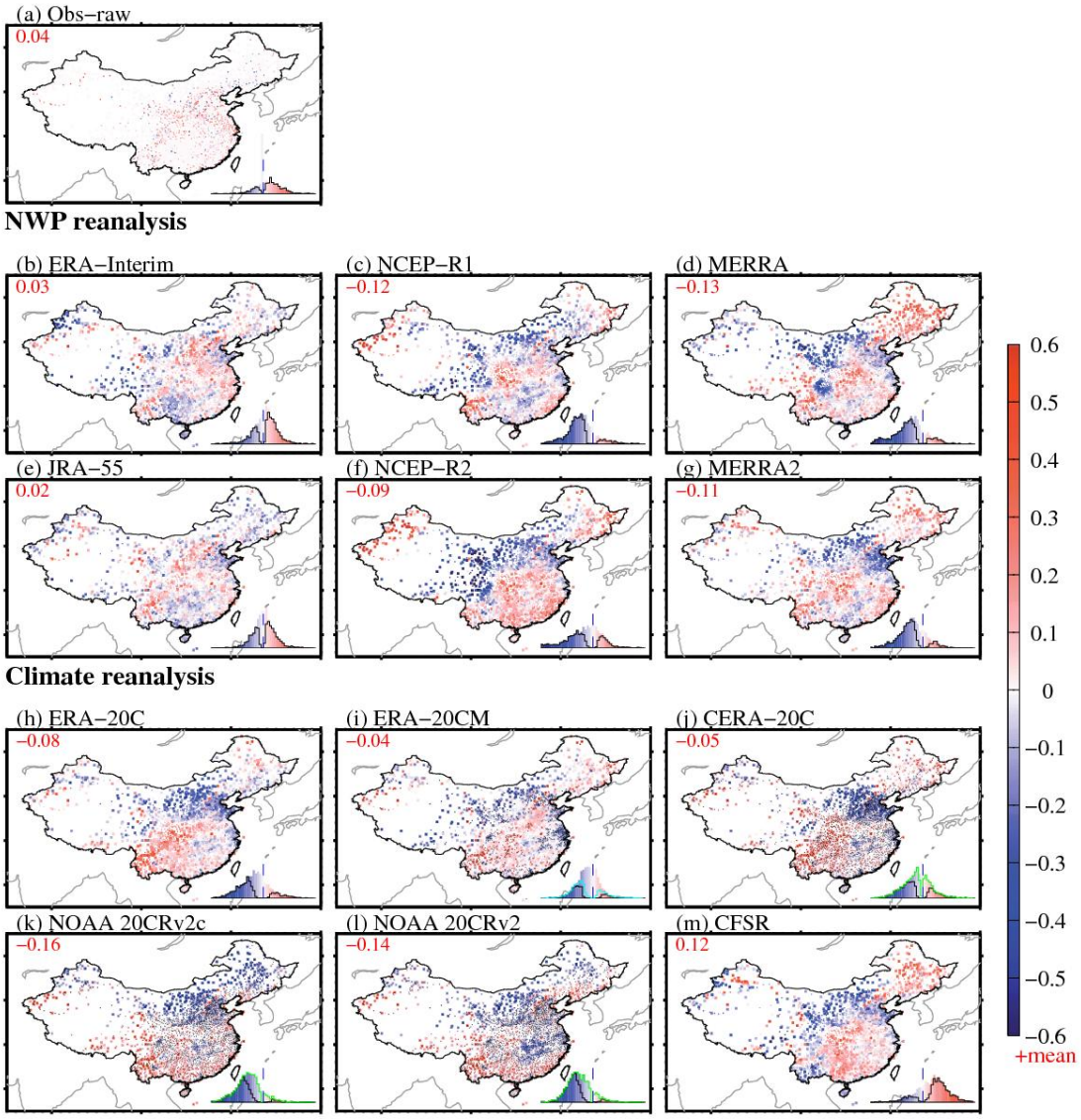


**Figure S7.** The same as Figure 5, but the colorbar is adjusted by adding mean value (in red number within each subfigure).

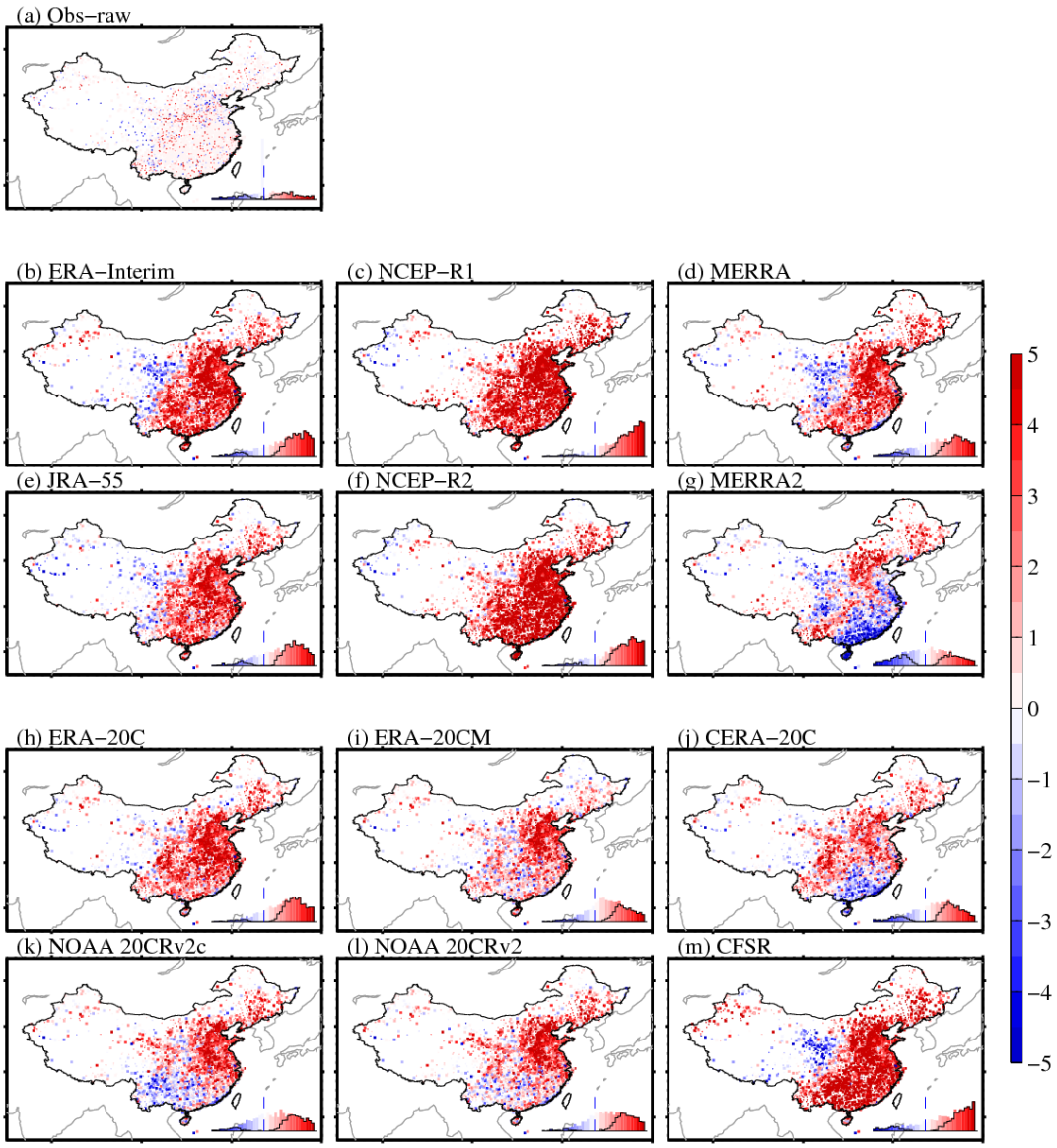


**Figure S8.** The simulated trend biases in surface incident solar radiation ($R_s$, unit: W·m$^{-2}$/decade) during the period 1979-2010 from the observations and the twelve reanalysis products over China. The probability distribution functions of all the trends are shown as colored histogram, and the black stairs are integrated from the trends with a significance level of 0.05 (based on two-tailed Student's *t*-test).

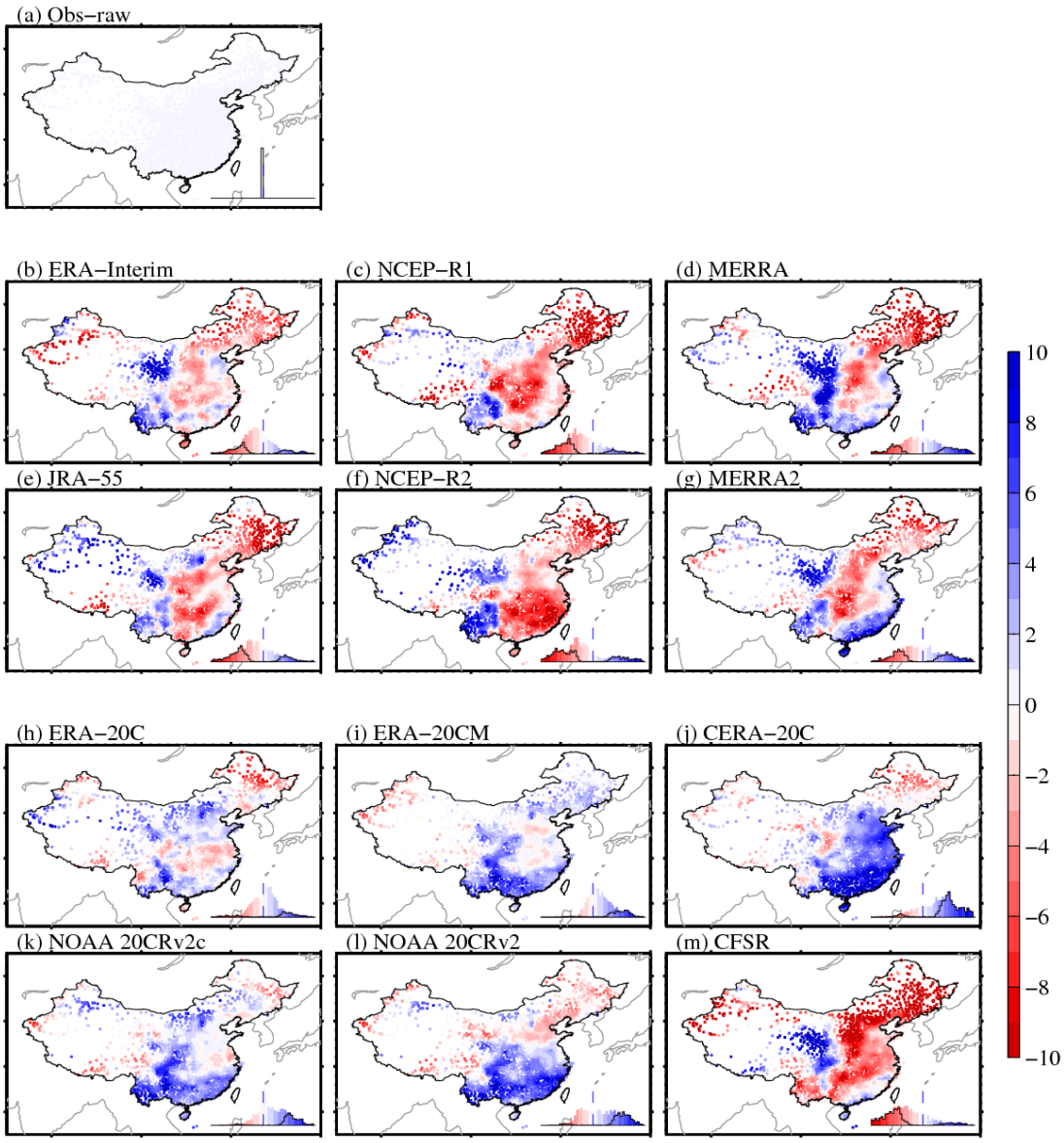


**Figure S9.** The simulated trend biases in the precipitation frequency (PF, unit: days/decade) during the period 1979-2010 from the observations and the twelve reanalysis products over China. The probability distribution functions of all the trends are shown as colored histogram, and the black stairs are integrated from the trends with a significance level of 0.05 (based on two-tailed Student's *t*-test).

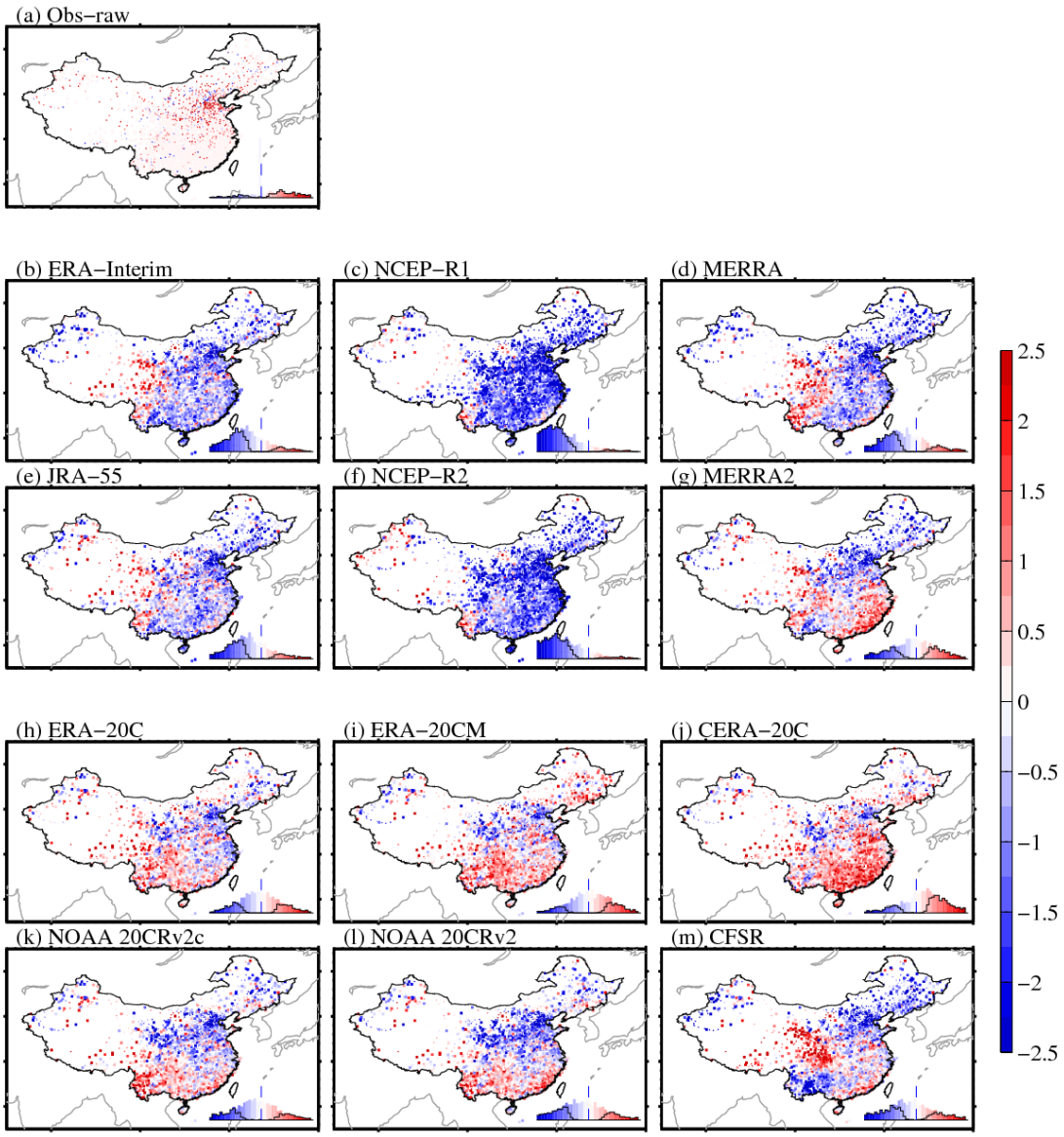


**Figure S10.** The simulated trend biases in surface downward longwave radiation ($L_d$, unit: W·m$^{-2}$/decade) during the period 1979-2010 from the observations and the twelve reanalysis products over China. The probability distribution functions of all the trends are shown as colored histogram, and the black stairs are integrated from the trends with a significance level of 0.05 (based on two-tailed Student's *t*-test).

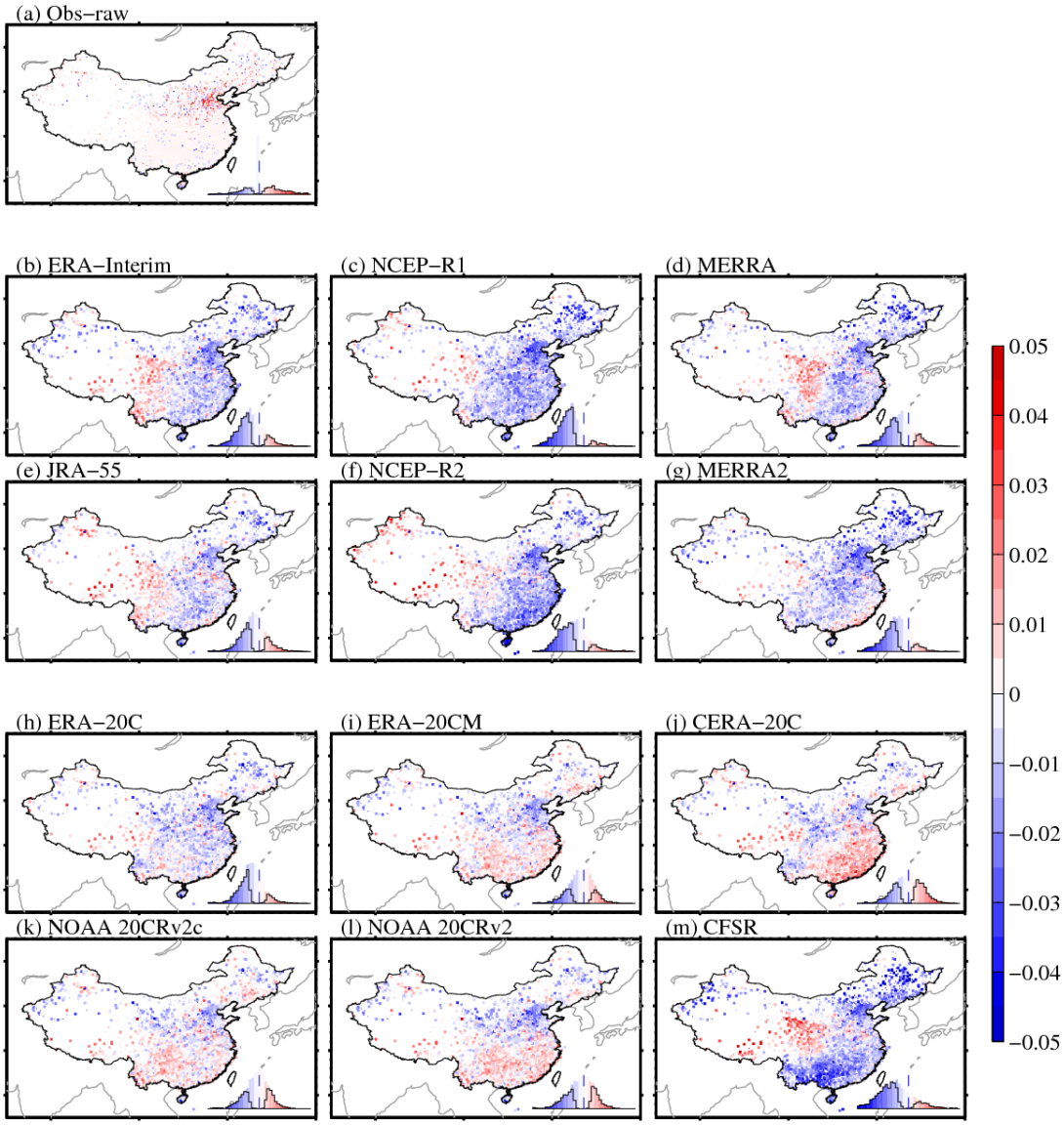


**Figure S11.** The simulated trend biases in cloud fraction (cld, unit: 1/decade) during the period 1979-2010 from the observations and the twelve reanalysis products over China. The probability distribution functions of all the trends are shown as colored histogram, and the black stairs are integrated from the trends with a significance level of 0.05 (based on two-tailed Student's *t*-test).

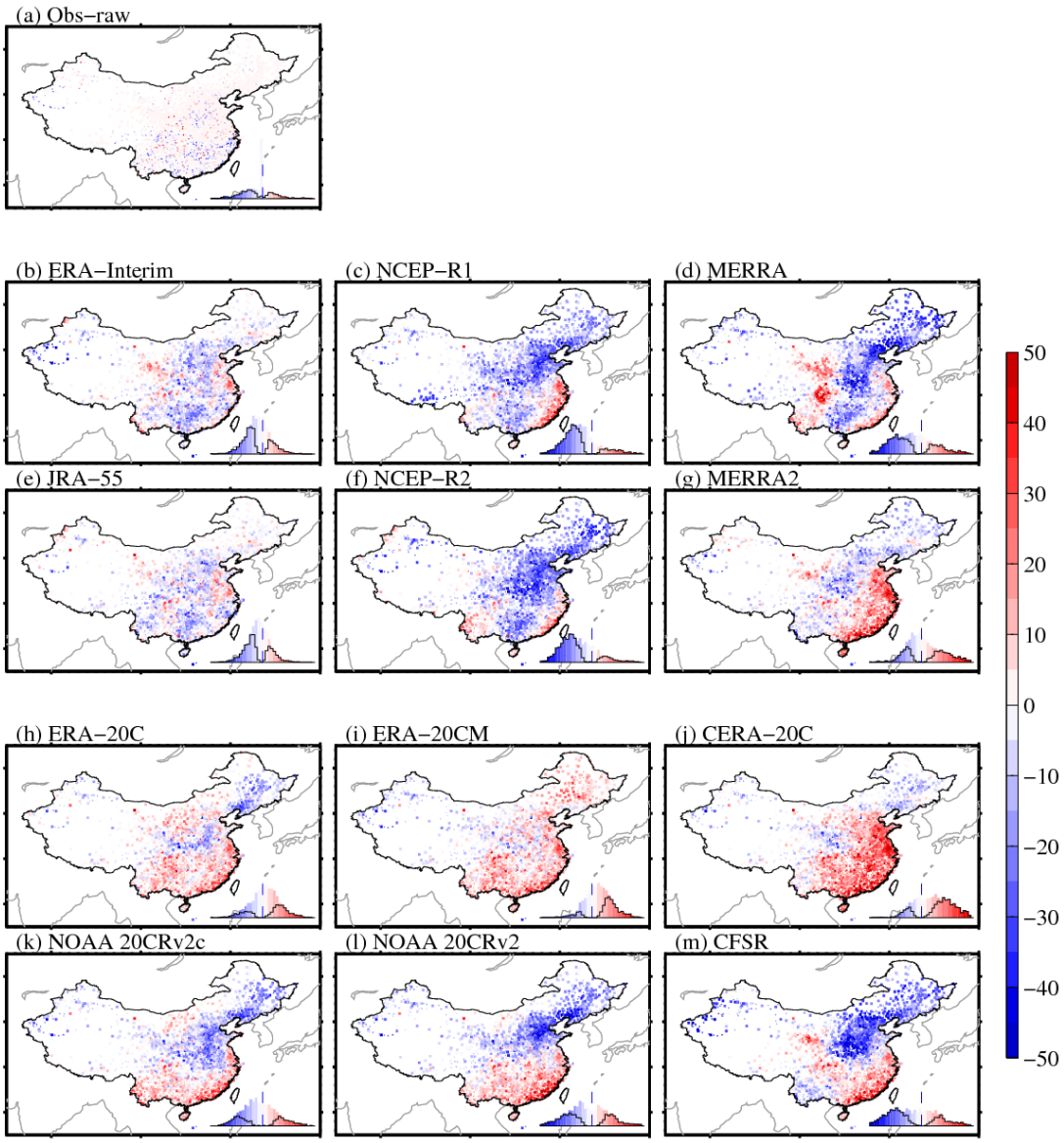


**Figure S12.** The simulated trend biases in the atmospheric water vapor (WVP, unit: Pa/decade) during the period 1979-2010 from the observations and the twelve reanalysis products over China. The probability distribution functions of all the trends are shown as colored histogram, and the black stairs are integrated from the trends with a significance level of 0.05 (based on two-tailed Student's *t*-test).

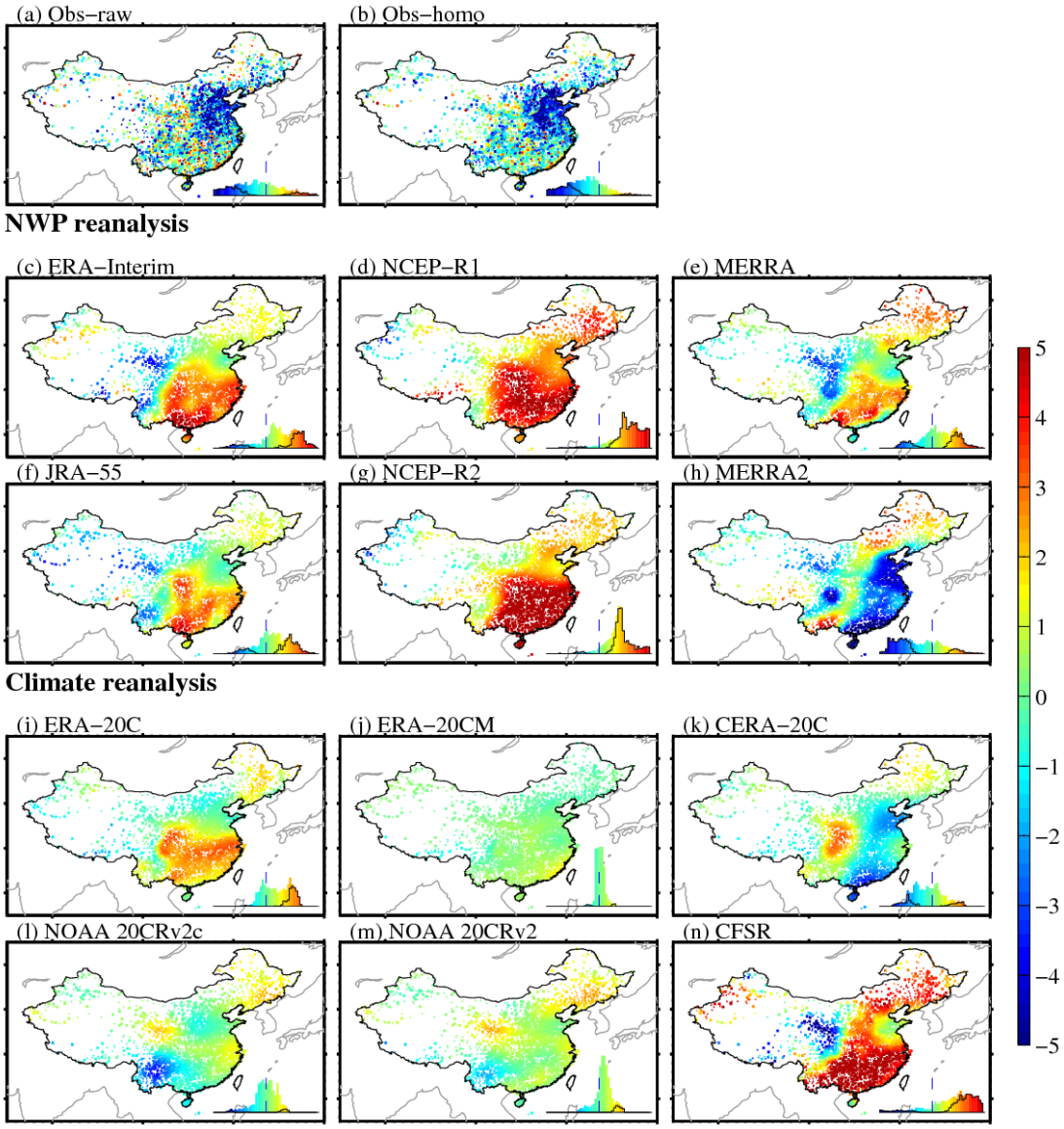


**Figure S13.** The trends in surface incident solar radiation ($R_s$, unit: W·m$^{-2}$/decade) during the period 1979-2010 from the observations and the twelve reanalysis products over China. The probability distribution functions of all the trends are shown as colored histogram, and the black stairs are integrated from the trends with a significance level of 0.05 (based on two-tailed Student's *t*-test).

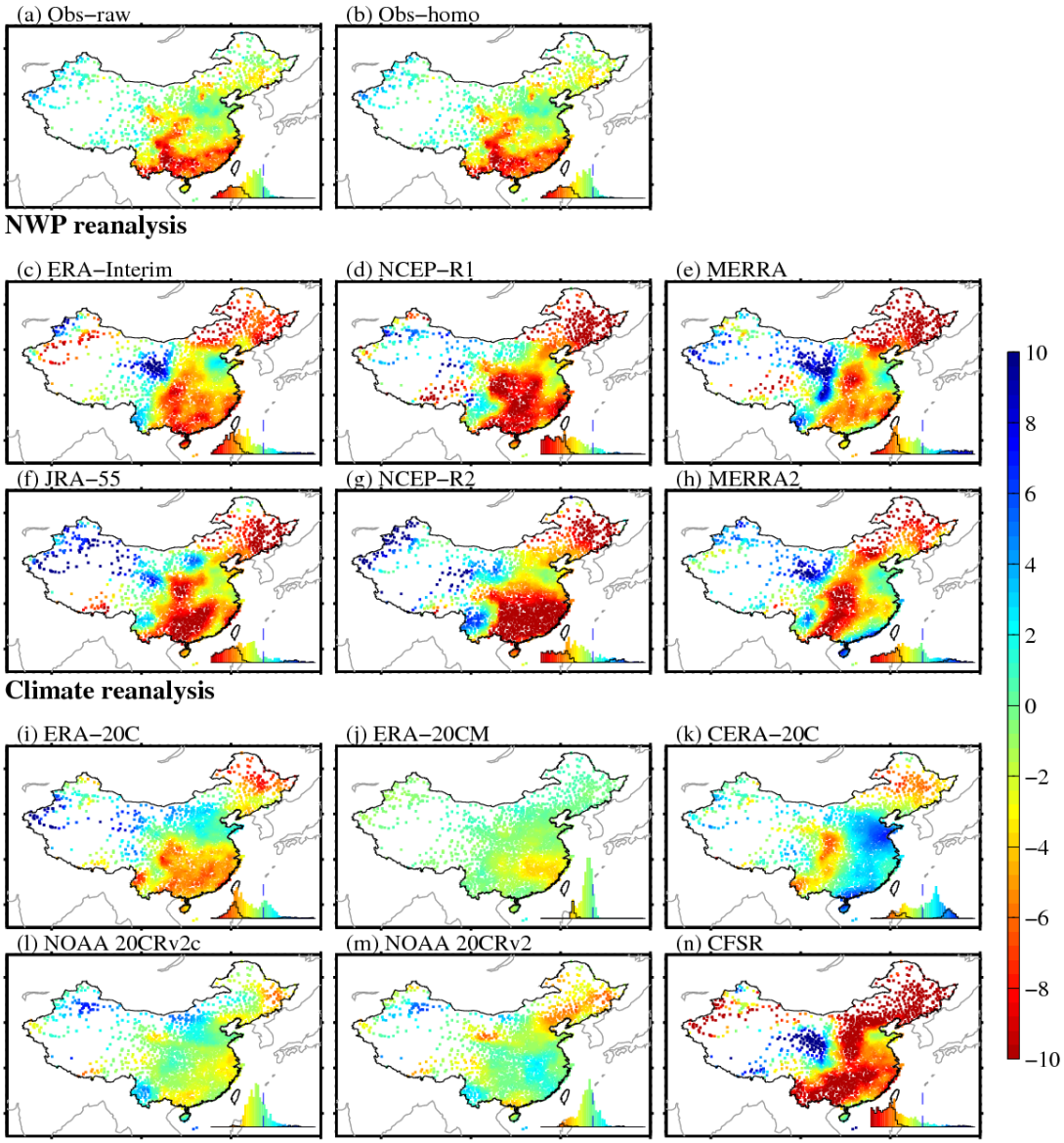


**Figure S14.** The trends in precipitation frequency (unit: days/decade) during the period 1979-2010 from the observations and the twelve reanalysis products over China. The probability distribution functions of all the trends are shown as colored histogram, and the black stairs are integrated from the trends with a significance level of 0.05 (based on two-tailed Student's *t*-test).

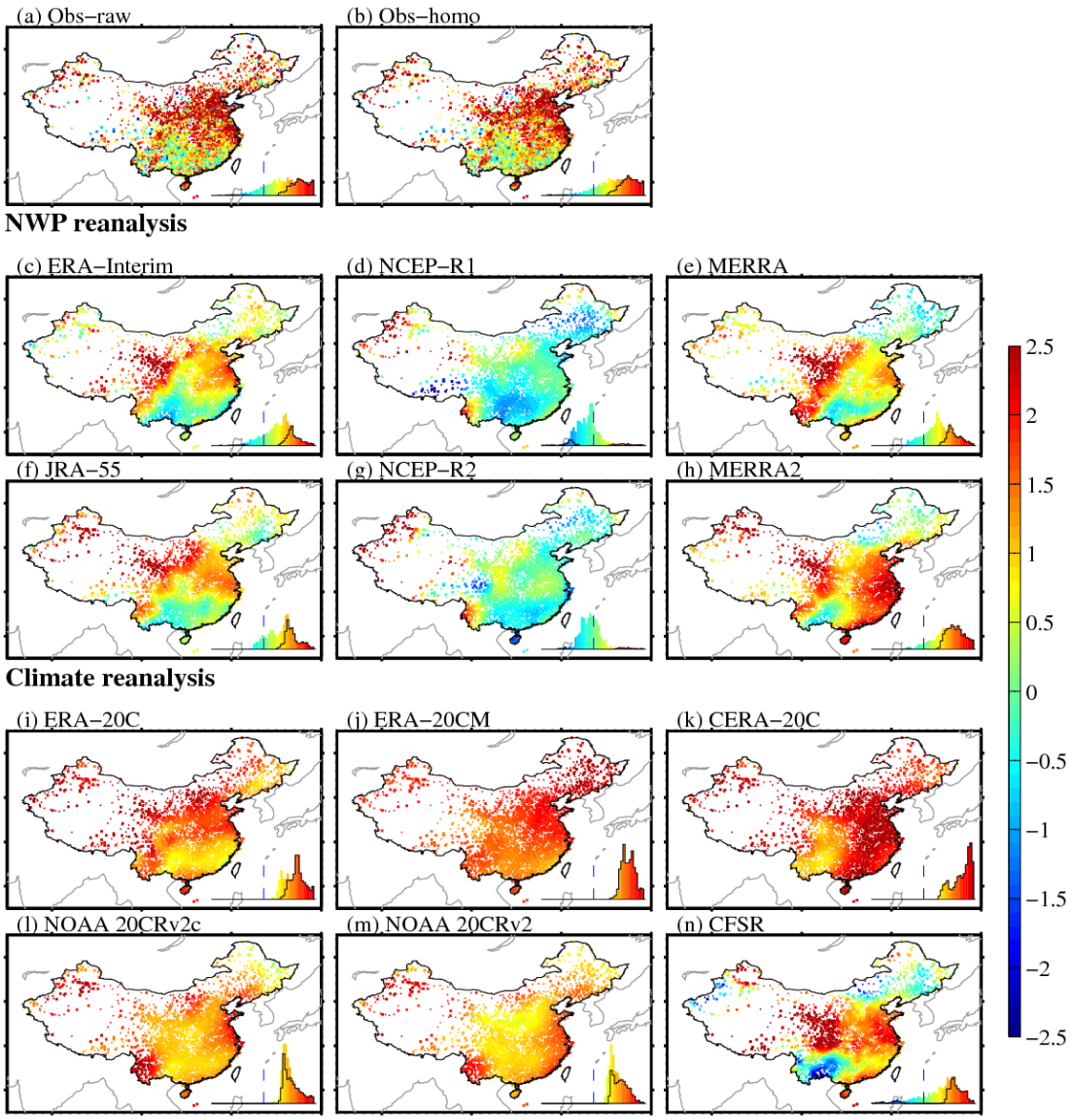


**Figure S15.** The trends in surface downward longwave radiation ($L_d$, unit: W·m$^{-2}$/decade) during the period 1979-2010 from the observations and the twelve reanalysis products over China. The probability distribution functions of all the trends are shown as colored histogram, and the black stairs are integrated from the trends with a significance level of 0.05 (based on two-tailed Student's *t*-test).

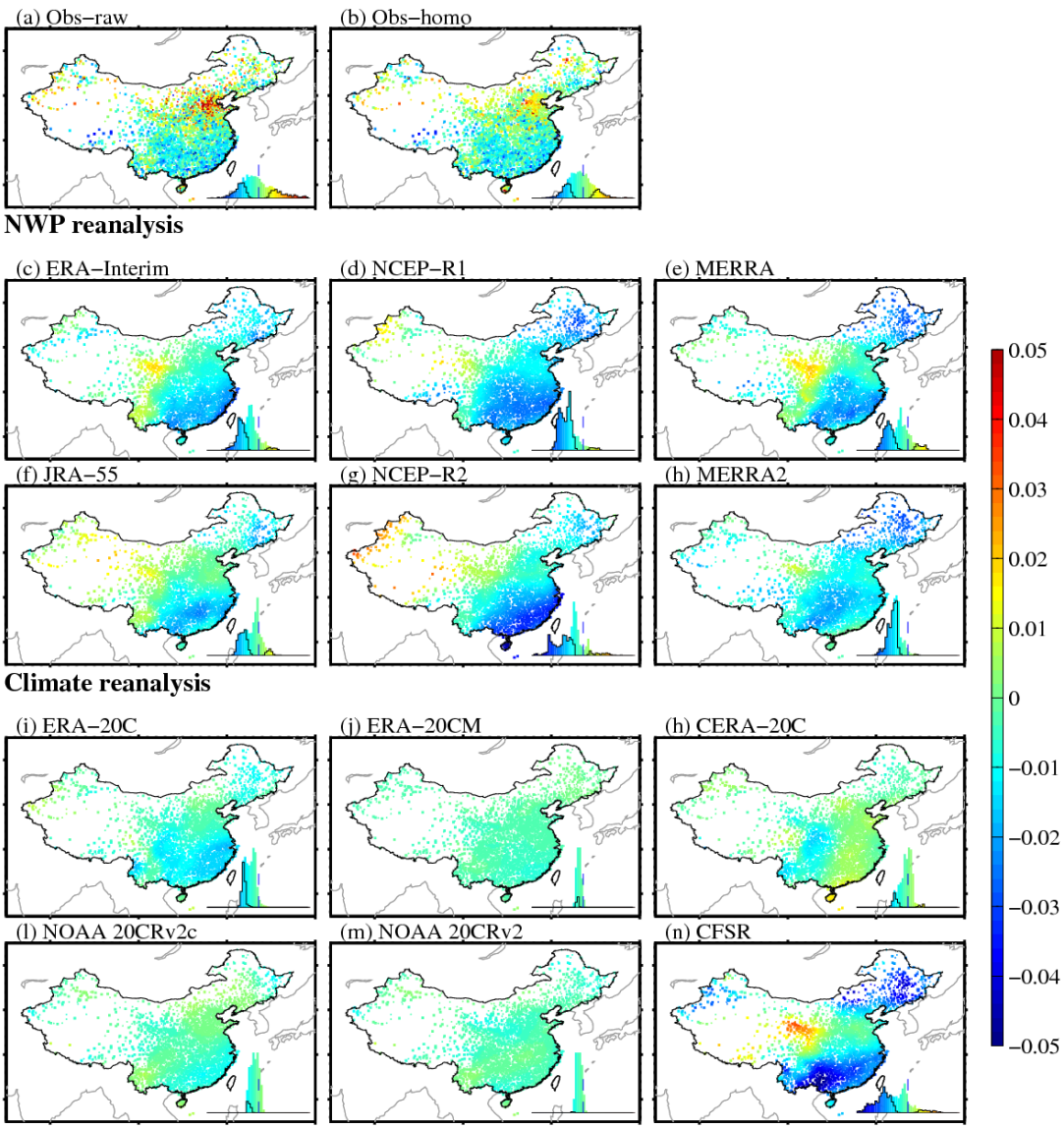


**Figure S16.** The trends in cloud fraction (cld, unit: 1/decade) during the period 1979-2010 from the observations and the twelve reanalysis products over China. The probability distribution functions of all the trends are shown as colored histogram, and the black stairs are integrated from the trends with a significance level of 0.05 (based on two-tailed Student's *t*-test).

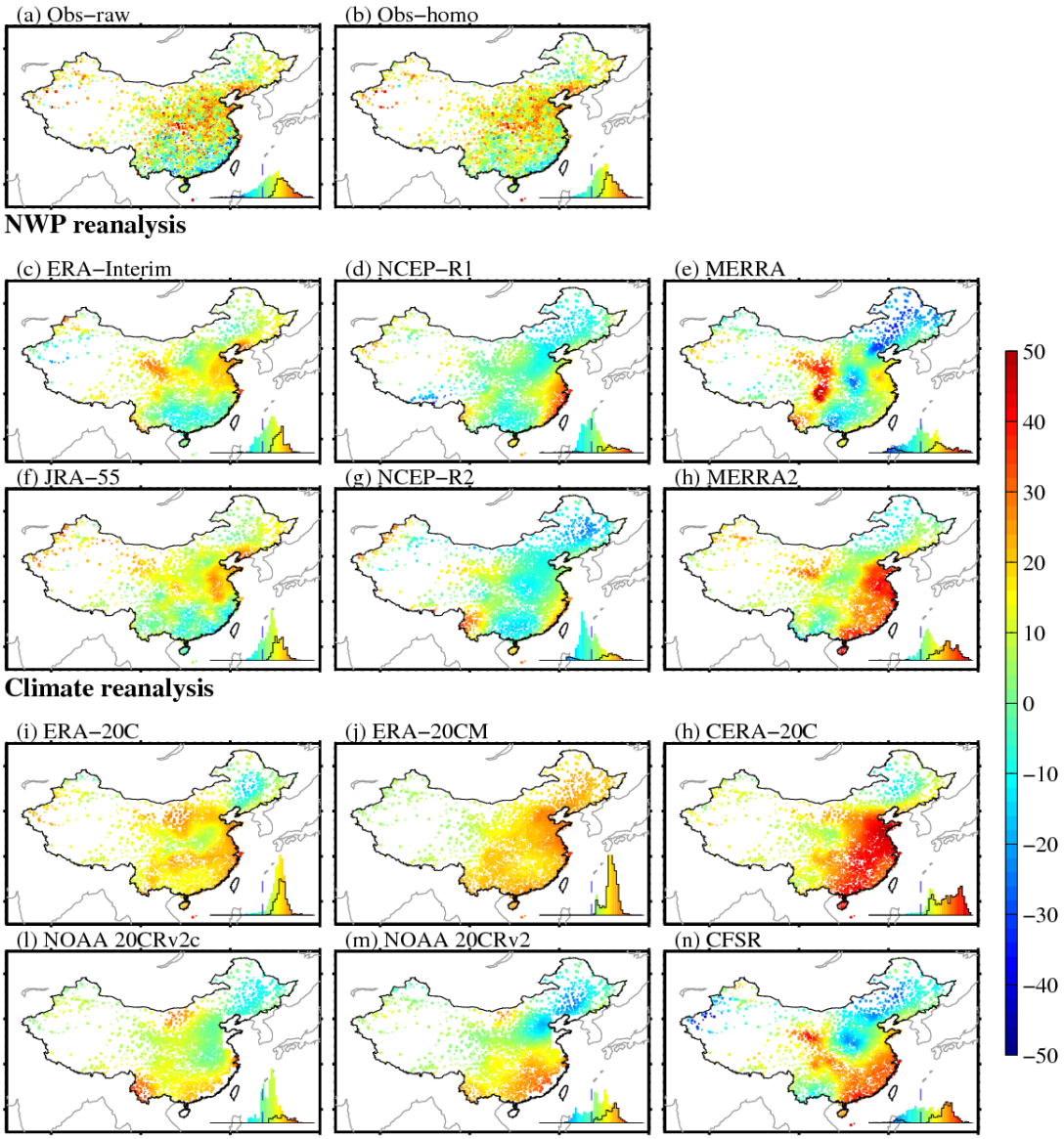


115

116 **Figure S17.** The trends in the atmospheric water vapor (WVP, unit: Pa/decade) during

117 the period 1979-2010 from the observations and the twelve reanalysis products over

118 China. The probability distribution functions of all the trends are shown as colored

119 histogram, and the black stairs are integrated from the trends with a significance level

120 of 0.05 (based on two-tailed Student's *t*-test).

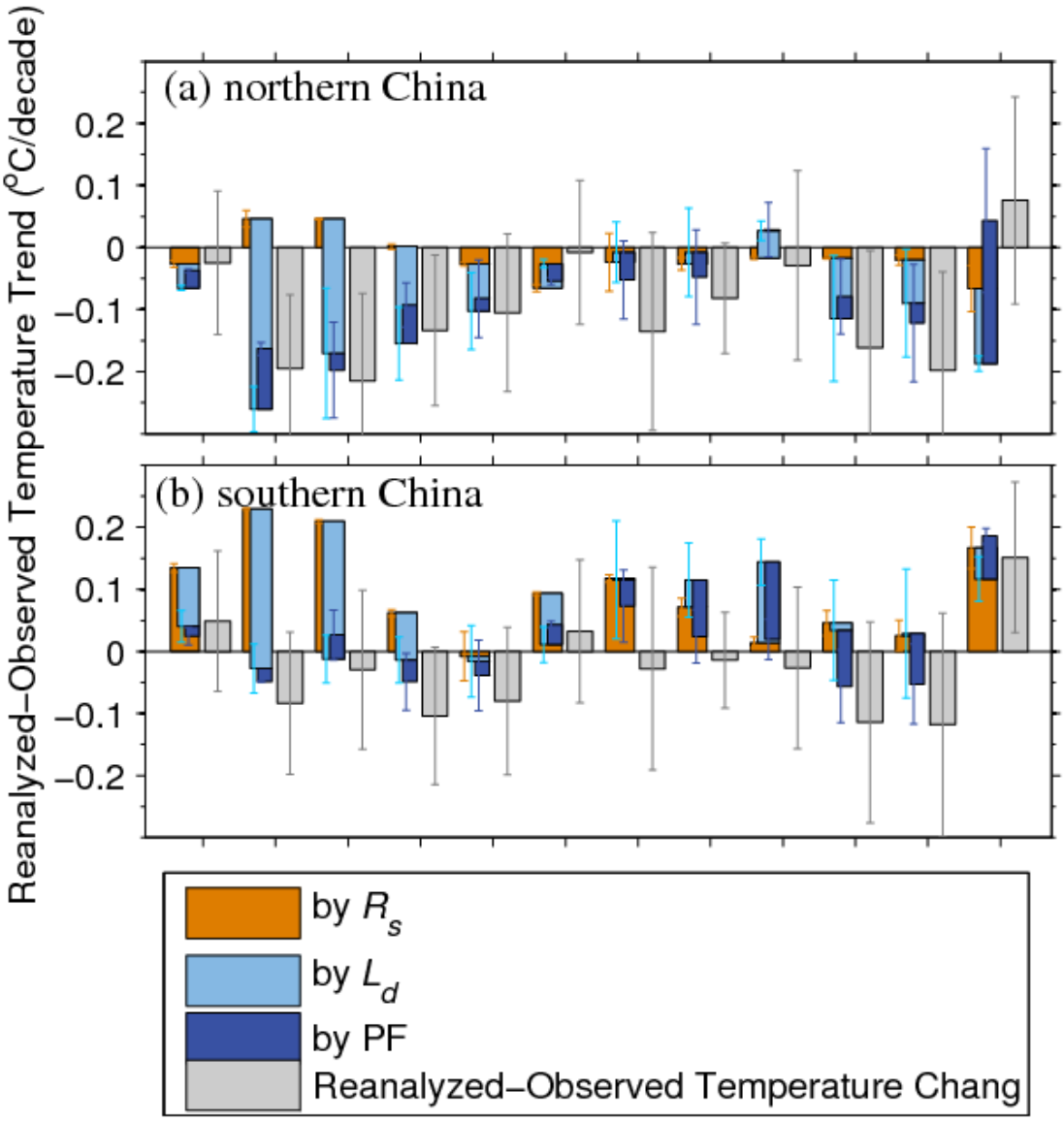


**Figure S18.** The same as Figure 7, but over northern China (including the Tibetan Plateau, Northwest China, Loess Plateau, Northeast China) and southern China (including the North China Plain, Middle China and Southeast China).

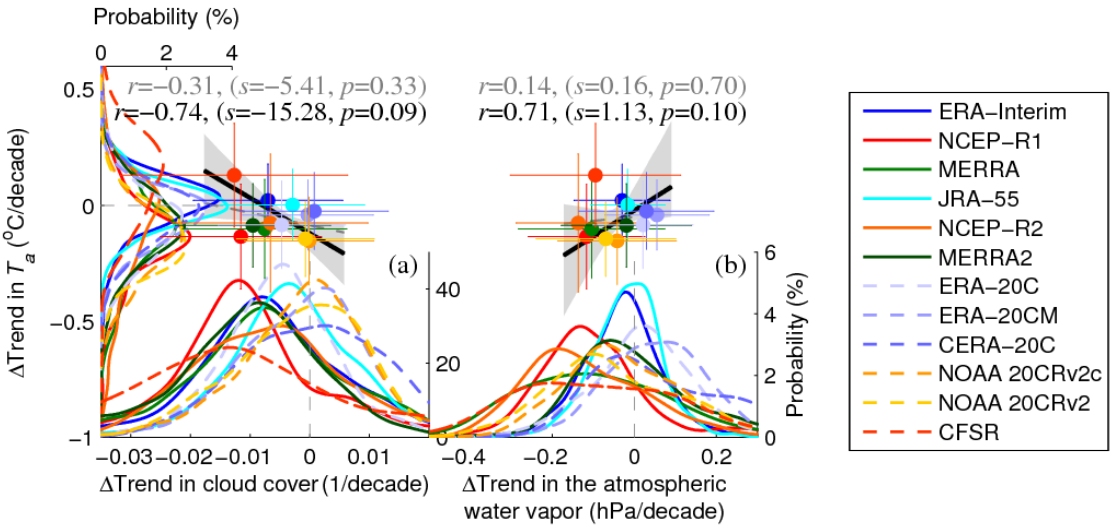


125

126 **Figure S19.** The same as Figure 8, but for the simulated biases in (**a**) cloud fraction

127 and (**b**) the atmospheric water vapor.

**Figure S20.** The same as Figure 8, but over China's subregions.

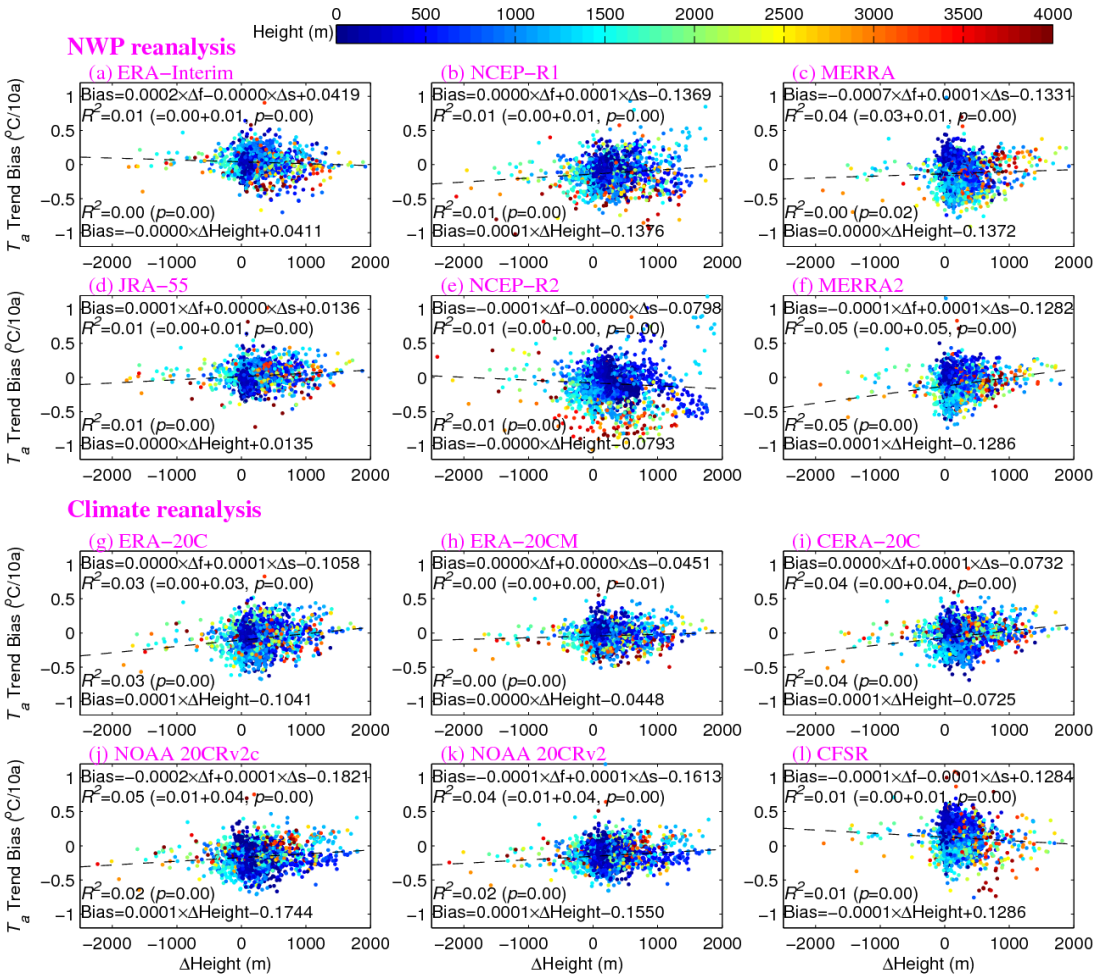


**Figure S21.** The same as Figure 2, but for the trend biases in surface air temperature ($T_a$, unit: ℃/decade). The elevation difference between model and stations actually influence the trend bias in $T_a$, but can not explain the spatial pattern in the trend bias in $T_a$ ($R^2$=0.02), mainly due to the nearest warming within the lowest atmospheric boundary layer. Moreover, compared the same-grid models (NOAA 20CRv2c vs. NOAA 20CRv2, MERRA vs. MERRA2, NCEP-R1 vs. NCEP-R2 and ERA-20C vs. ERA-20CM), we found the one statistically correlates with the elevation difference but the other does not, which implies that this statistical correlation should not be physical significance. Additionally, the elevation difference does not change with time.

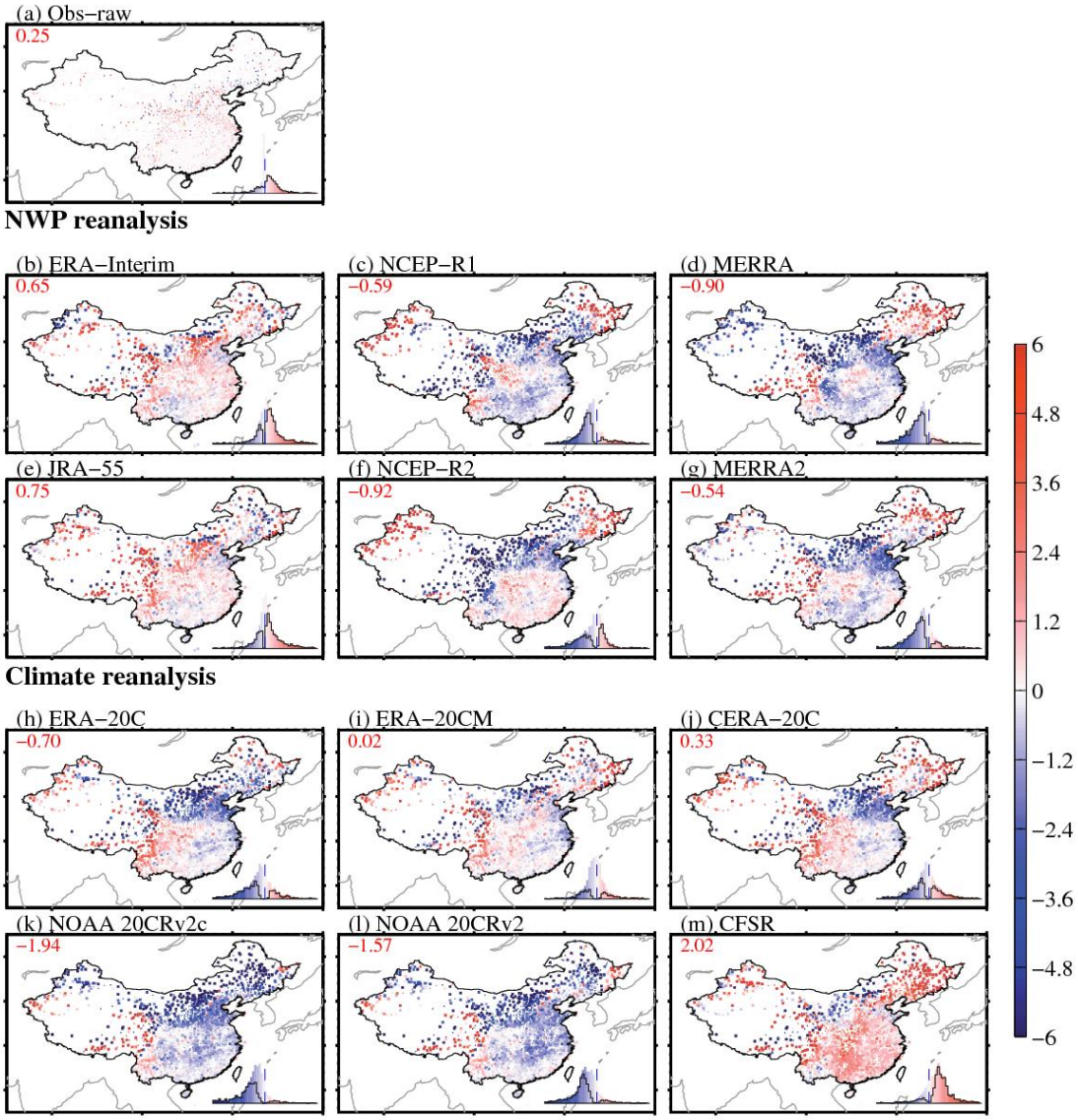


141

142 **Figure S22.** The same as Figure 5, but for the normalized trends in surface air
143 temperature (%/decade). The normalized trends can exclude the impact of absolute
144 value of temperature on the trends. One can find that the spatial patterns in the
145 normalized trends is very near to those of the trends, implying the impact of
146 difference in absolute value of temperature due to the site-to-grid inconsistency can be
147 neglected. This result is consistent with that based on Figure S20.

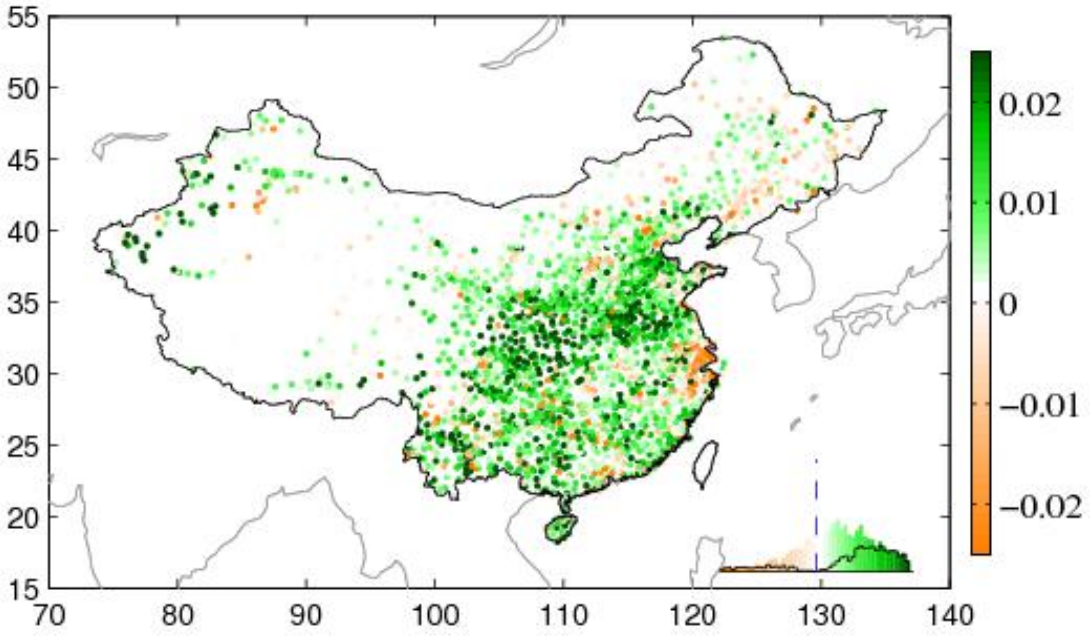


**Figure S23.** The trend in vegetation growth depicted by Normalized Difference Vegetation Index (NDVI, unit: 1/decade) during the period 1981-2010 from the observations and the twelve reanalysis products over China. The probability distribution functions of all the trends are shown as colored histogram, and the black stairs are integrated from the trends with a significance level of 0.05 (based on two-tailed Student's *t*-test).